

Superior ultra-transparent broadband terahertz polarizers by nanoimprint lithography

Alexandre Chicharo*, Tatiana G. Rappoport, Chun-Da Liao, Jérôme Borme, Nuno M. R. Peres, Pedro Alpuim

ABSTRACT: We report the largest broadband terahertz (THz) polarizer based on a flexible ultra-transparent cyclic olefin copolymer (COC). The COC polarizers were fabricated by nanoimprint soft lithography with the lowest reported pitch of 2 or 3 μm and depth of 3 μm and sub-wavelength Au bilayer wire grid. Fourier Transform Infrared spectroscopy in a large range of 0.9 -20 THz shows transmittance of bulk materials such as doped and undoped Si and polymers. COC polarizers present more than doubled transmission intensity and larger transmitting band when compared to Si. COC polarizers present superior performance when compared to Si polarizers, with extinctions ratios of at least 4.4 dB higher and registered performance supported by numerical simulations. Fabricated Si and COC polarizers' show larger operation gap when compared to a commercial polarizer. Fabrication of these polarizers can be easily up-scaled which certainly meets functional requirements for many THz devices and applications, such as high transparency, lower cost fabrication and flexible material.

KEYWORDS: Terahertz, Polarizer, Nanoimprint lithography, Fourier-transform infrared spectroscopy, Thin films, Cyclic olefin copolymer

The far-infrared (FIR) and particularly the terahertz (THz) region of the electromagnetic spectrum was often described as the final unexplored region of the electromagnetic wave spectrum.¹ Recently, THz-based technologies have seen significant developments.² This technology's main applications include imaging in astronomy, spectroscopic techniques, detection of chemicals or explosives, security screening, wide broadband wireless data communication, dry food inspection, etc.² Thus, in the past decades, many devices were developed such as THz emitters, detectors, and passive components such as lenses, filters, attenuators, and polarizers. In particular, polarizers are essential tools in spectroscopy. These devices manipulate the polarization degree of freedom of THz electromagnetic waves. Principally, linear polarizers are designed to separate light into two perpendicular polarization directions.³ The linearly polarized component is transmitted, and the other component is either reflected or absorbed.

Different kinds of THz polarizers have been developed based on different methods such as triangular Ag-film grating,⁴ carbon nanotube,⁵ Brewster's angle polarizers (BAPs),⁶ liquid crystal polarizers (LCPs),⁷ and wire-grid polarizers (WGPs).⁸⁻¹⁵ WGPs are widely adopted devices as THz polarizers due to a more controlled fabrication. They are typically composed of a material transparent in this spectrum region and a metallic wire grid configuration, i.e., an array of metal lines with a sub-wavelength period. When THz is irradiated onto the wire grid polarizer, the conductive electrons in the wires are driven by the electric field along its length.³ Light is transmitted in a direction in which electrons' movement is restricted and reflected in a direction in which electrons can move freely, i.e., the transmitted light is the transverse magnetic (TM) portion of the light, which has the electric field perpendicular to the wires. In contrast, transverse electric (TE) polarized light, which has the electric field paralleled to wires, is reflected, as depicted in Figure 1.

Many parameters can affect the optical properties of wire-grid THz polarizers, such as materials used for the substrate, materials used in conductive wires, the thickness of these materials, the pitch of the wires, the filling factor, and improved geometries of single or multiple wire grid in the same device. The figure of merit that determines the performance of polarizers is the extinction ratio (ER), i.e., the quotient between the transmitted light and the reflected light [ER dB = $10 \cdot \log(\text{TM}/\text{TE})$]. WGP in spectroscopy can cover a broad range of spectrum from ultraviolet, visible, infrared, and THz.³ Polarizers for the THz range have seen significant progress, such as an increase in transmitted light and extinction ratio, and the method for its polarization can be tailored for a given application.

Typical THz polarizer characterization is performed with THz spectroscopy in the time domain (THz-TDS).¹⁶ THz spectroscopy is a sensitive, high spectral resolution technique to measure both the amplitude and phase of THz pulses, typically in a narrow frequency range of 0.1 - 3 THz.³ An alternative method for characterization is performed using standard Fourier transform infrared spectroscopy (FTIR), capable of acquiring a broader spectrum of 0.9 - 20 THz. For studies in the THz, FTIR is typically coupled

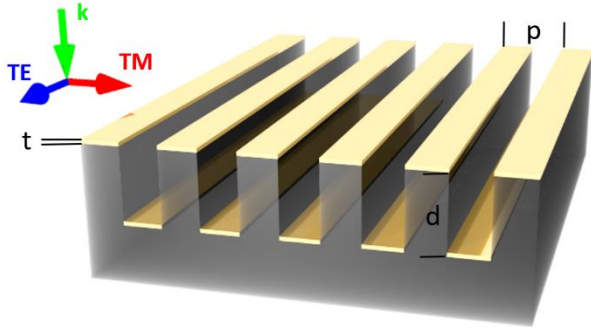


Figure 1. Schematic diagram of the double wire grid polarizer (DWGP). d : metal layer spacing; p : wire-grid pitch; t : metal layer thickness; fill factor is 50%; Green arrow indicates the direction of incident light and the red and blue arrows represent the electric field component of the electromagnetic radiation. The red arrow indicates the transmitted transverse magnetic (TM) light and blue arrow

with a mercury discharge lamp, providing a continuous far-infrared light source exposing the materials. THz-TDS and FTIR are adequate characterization techniques with complementary spectral information of WGP in the THz range. Nonetheless, FTIR presents sensitivity problems when acquiring very low transmitted TE, which may limit WGP characterization of the observed spectrum.

Several methods have been pursued for the fabrication of WGP. Some commercial polarizers are composed of free-standing metal grids. These are standing grids in air/vacuum and show low TM loss; however, fabrication of well-aligned wires is challenging for low pitches $<5 \mu\text{m}$.⁸ Alternative methods employ inkjet printing method with a conductive material such as silver-nanoparticle ink on a Kapton film.⁹ Although this process has a short manufacturing time, additional optimization with this method is required to reduce pitches below $40 \mu\text{m}$ and improve the reproducibility of the printed material. More modern polarizers are composed of a monolayer of wire grid of metals on a substrate providing more resistance for thinner wires. This is obtained through cleanroom standard photolithography techniques, sputtering/electroplating/evaporation of metals, and, combined, etch or lift-off techniques to pattern the micron-sized wires.³ Typical substrate for these polarizers is Si wafers, which offer fair transmission in THz range and is a standard material used in the semiconductor industry, chosen also for its mass production capability. In particular, it's known that undoped float zone Si presents higher transmittance when compared to doped Si wafer. Other substrate materials for WGP were also demonstrated with improved transmissions such as polycarbonate,¹² sapphire,^{5,17} polyethylene terephthalate (PET) film,¹⁰ and cyclic olefin polymer (COP).¹³ The extinction ratios on these WGP devices are very high, typically vary from 20 – 60 dB.³

An improved geometry for WGP was proposed in the 70s composed of a double wire grid polarizer (DWGP) in a range of 0.1 – 1 THz.¹⁸ Its structure combines a bottom grid aligned with a top grid with sub-wavelength slits. These realize mirrors for THz frequencies with the use of one-dimensional metal reflectivity. Two grids were combined to form a Fabry-Pérot (FP) filter, which features the corresponding transmission bands.¹⁹ More recently, further theoretical analysis led to designing a polarizer with a very high extinction ratio in the 0.3 – 3 THz region and composed of two dense metal wire gratings in parallel of which the grating pitch is much smaller than the incident wavelength.²⁰ This method utilizes FP interference effect and polarization-sensitive response of metal wire gratings. Numerically simulations show a very high extinction ratio polarizer of around 180 dB. Fabrication of this type

of device with two aligned small metal grids is challenging, especially for low pitches. An interesting DWGP approach was proposed with the top layer misaligned with the bottom layer, as depicted in Figure 1.¹⁴ A simple fabrication approach was demonstrated on a Si substrate with three steps: lithography patterning, dry silicon etching, and a self-aligned gold deposition of two grids. The maximum extinction ratio of this DWGP was record of 69.9 dB at 1.67 THz, with a pitch of $4 \mu\text{m}$, depth of $5 \mu\text{m}$, and a gold thickness of $0.4 \mu\text{m}$.³ The work compares fabricated devices composed of WGP and DWGP, showing that the latter have TE transmittances of three orders of magnitude lower than those of WGP and thus three times higher ER.

This DWGP's geometry shows excellent potential for a commercial THz polarizer. With this purpose in mind, in this work, we pushed the limits of DWGP to provide a next-generation THz linear polarizers. We investigate different materials with enhanced transmission properties and propose a new fabrication method, such as nanoimprint lithography. This technique is still aligned with low-cost requirements and upscaling fabrication capability for new potential THz markets. Performing numerical simulations, we investigated different parameters to improve DWGP characteristics and to predict fabricated devices' best performance. These include the substrate material, pitch (p), depth of the bilayer wire grids (d), and the metal thickness (t), as depicted in Figure 1. We then characterize the fabricated polarizers using a FTIR equipment with a broad spectrum, not yet explored in past works with THz polarizers.

EXPERIMENTAL SECTION

Material selection

Silicon wafer is a well-known material for its opacity in the visible and fair transparency in THz range.^{21–23} Due to its prevalent use in the semiconductor industry, it is a strong candidate for passive THz optical components. Other inorganic materials are also used with good optical properties in this band, such as diamond, crystal quartz, and sapphire.^{21,22} These materials are transparent in the visible region; however, quartz is a birefringent material, and diamond and sapphire are too expensive materials for large production. Additionally, crystalline materials typically have lower transmittance values in the THz band because of losses from reflection.²³ Another uprising class of materials showing good performance in the THz region are polymers.^{21,23–25} Among a large variety of polymers with excellent THz transparencies and low reflectivity are polymethylpentene (TPX), high-density polyethylene (HDPE), polyethylene terephthalate (PET), cyclic olefin polymer (COP), and cyclic olefin copolymer (COC). PET, however, presents a higher absorption coefficient in this range.¹⁰ COP and COC stand out as unique materials as they show a higher Young Modulus, i.e., are more resilient and can be made thinner without breaking when compared to HPDE and TPX.^{13,26,27} These materials have a constant refractive index of 1.53-1.54 from THz up to the visible range, high chemical resistance to hydrolysis, acids, alkalis, and polar solvents, present low birefringence, and have excellent gas barrier properties.^{26,27} A particular kind of commercial COP is Tsurupica® or Picarin®, often used in THz lenses.²³

In the pursuit of enhancing THz polarizers' performance, we analyzed room temperature transmission of several materials using FTIR spectroscopy in a broadband range of 0.9-20 THz. Two types of Si wafers (undoped and p-doped) and two kinds of polymer sheets (COP and COC) were inspected (section S1 of Supporting Information). Figure 2 a) shows the transmittance spectra for the four selected materials (section S2 of Supporting Information).

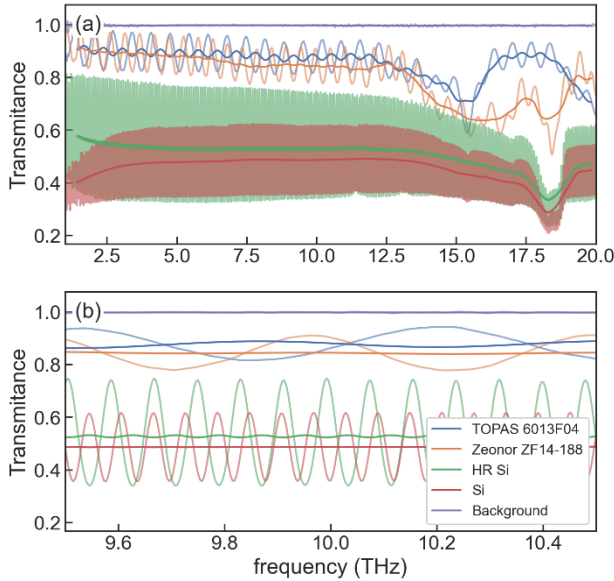


Figure 3. (a) Transmission spectra of undoped SSP Si, doped DSP HR Si, COP polymer (Zeonor®), and COC polymer (TOPAS®) in transparent fringe lines. Solid lines are the moving geometric mean of measured fringe patterns in the same color. (b) Zoom-in of the average and fringe pattern of materials near 10 THz.

Both polymers have improved optical transmittance in the THz range when compared to the Si wafer substrates. Undoped high resistive (HR) Si presents slightly higher transparency than p-doped wafers, particularly at lower frequencies. High-resolution spectra (1 cm^{-1}) of all these materials show a typical fringe pattern.²² Figure 2b) shows a zoom-in fringe pattern at around 10 THz. These fringes can be explained by Fabry-Pérot interference between multiple reflections of light from the two reflecting surfaces of the material.²⁸ It is well known that the thickness of the films, t_F , can be obtained from this fringe pattern. Thickness is inversely proportional to the mean distance of the interference maxima, Δf , within a selected frequency range, and from the refractive index n of the film, considered constant in that interval: $t_F = 1/(2 \cdot n \cdot \Delta f)$.²⁹ Thicker materials and high refractive indexes present higher frequency fringes, as can be seen comparing the spectra of both Si wafers, where nominal thickness specifications are $725 \mu\text{m}$ and $525 \mu\text{m}$ for the doped and HR wafer, respectively. The different polishing of these samples can explain the lower fringe amplitude in the doped Si sample compared to the undoped Si sample: the doped Si is single-side polished (SSP), and thus internal reflection is reduced when compared to undoped double side polished (DSP). COP and COC samples are thinner (nominal $188 \mu\text{m}$ and $140 \mu\text{m}$, respectively) with lower refractive indexes and show lower frequency fringes than Si samples. The thickness of the substrates was calculated with FTIR software OPUS v8, considering refractive indices of Si and COC/COP substrates of 3.42 and 1.53, respectively, in the frequency range of 3 to 12 THz. The calculated layer thicknesses, t_F , are close to reference values: $708.11 \mu\text{m}$ and $539.42 \mu\text{m}$ respectively for doped and undoped Si; $185.67 \mu\text{m}$ for COP and $142.97 \mu\text{m}$ COC substrate.

The observed fringe pattern is not critical in polarizers' performance. Typically, spectroscopic techniques rely on removing the background pattern of overall systems' components such as light intensity over the spectra, internal reflections, etc. For simplicity and easier comparison to simulated models, each material's spectral fringes' average intensity was obtained, as described in the Experimental Methods section (section S3 of Supporting Information). In

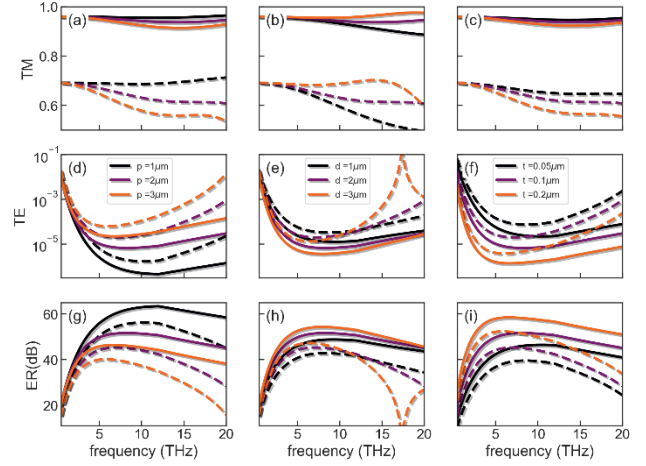


Figure 2 Dependence of the performance of double grating polarizers DWGP in COC (continuous line) and doped Si (dashed lines). First column (a,d,g) simulations have fixed depth and thickness ($d = 2 \mu\text{m}$, $t = 0.1 \mu\text{m}$), second column (b,e,h) has fixed pitch and thickness ($p = 2 \mu\text{m}$, $t = 0.1 \mu\text{m}$), and third column (c,f,i) has fixed pitch and depth ($p = 2 \mu\text{m}$ and $d = 3 \mu\text{m}$).

the simulation models, FP fringes were not included to simplify the performance analysis of fabricated devices.

We observe that undoped Si has a slightly higher transmission than doped Si, as previously shown.²³ Average values of 52.7% and 48.6% for undoped and doped Si, respectively, were obtained at around 10 THz. In both these spectra, an absorbent peak was observed at about 19 THz.²² COP and COC films show a much higher transparency over the full range, with average values around 10 THz of 86.4% and 87.5%, respectively. Figure 2a) shows that COC presents slightly higher transmission than COP and thus was chosen in subsequent simulation and fabrication of polarizers.

A conducting material is used for the grid in WGP. Several materials could be used, such as gold (Au), aluminum (Al), silver (Ag), copper (Cu), and indium tin oxide (ITO). Ag and Al are ideal because they present the highest absolute complex refractive indices n and k in the far infrared.⁴ However, Ag tends to oxidize over time, and sputtering of high-quality Al is more challenging. ITO stands as a transparent conducting oxide material, however, its relatively low conductivity requires thicker films.¹⁰ Due to long-term chemical stability, large absolute value of complex refractive index,³⁰ and standard sputtering recipe, Au was chosen as the material for the metal-grating films in this work.

Simulation of polarizers

In the pursuit of enhancing current THz polarizers and increasing their transparency in the THz range using new high-potential materials, theoretical simulations were performed, based on the DWGP configuration depicted in Figure 1. Three main parameters were inspected: *i*) pitch of the grating (p); *ii*) depth of the grating (d); and *iii*) the thickness of the gold layer (t). Figure 3 shows a simulation of devices made of doped Si (dashed lines) and COC (continuous line) for each set of parameters p , d , and t for transmitted light TM, TE, and corresponding ER. All pitches p have a fill factor of 0.5. The first column [Figure 3 a), d), and g)] has fixed $d = 2 \mu\text{m}$ and $t = 0.1 \mu\text{m}$, the second column [Figure 3 b), e) and g)] has fixed $p = 2 \mu\text{m}$ and $t = 0.1 \mu\text{m}$, and the third column [Figure 3

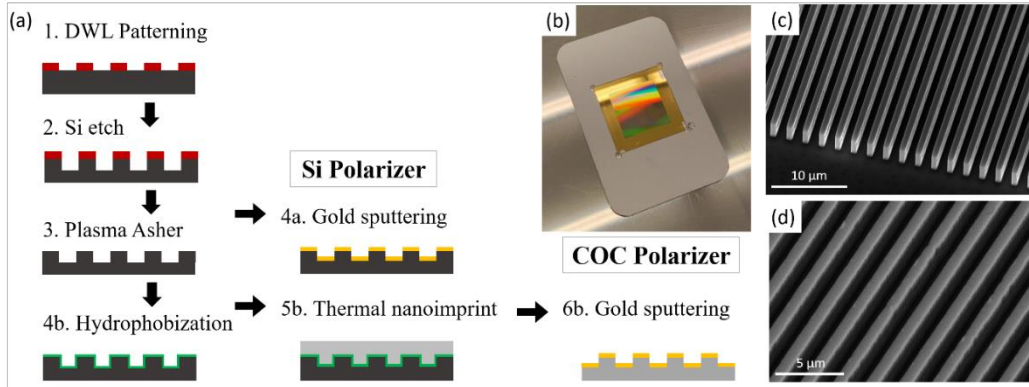


Figure 4. (a) Fabrication steps for Si (black) and COC (grey) double-layer wire grid polarizers (DWGP). Materials used are photoresist (red), thin layer hydrophobic agent (green), and gold layer (yellow). (b) COC DWGP in the alignment support. (c) SEM image of Si DWGP after step 4a. d) SEM image of COC DWGP after step 6b.

c), f) and i)] has fixed $p = 2 \mu\text{m}$ and $d = 2 \mu\text{m}$. Simulations were performed in COMSOL software using refractive indexes of 3.5 for Si and 1.4 for COC polymer, and, optical dielectric function of gold was interpolated from a broad range of experimental data (section S4 of Supporting Information).

As observed in the set of the first row [Figure 3 a), b), and c)], transmitted TM light is at least 40% higher in COC devices than in doped Si ones over the entire spectrum. Additionally, the TE component is less transmitted in COC devices than in Si DWGP, as observed in the second row, Figure 3 d), e), and f). Consequently, the ER, in the third row, is highly improved in the COC compared with the Si DWGP polarizers, as seen in Figure 3 g), h), and i). It is also observed that decreasing p increases the overall TM over the full spectra, decreases TE, and increases ER for both materials. In particular, transmitted TM in COC is not much affected by p compared to Si because an increasing p in Si devices leads to loss in TM at higher frequencies. When studying variations in devices' depth d , the second column shows an overall higher COC device performance than for Si ones. Nonetheless, higher d leads to better performance in COC devices as seen by higher TM and ER for the full spectra analyzed. When observing different gold thicknesses, we can see a small decrease in TM and higher TE loss in both materials, particularly for higher frequencies. A thicker gold layer leads to overall better performance in ER, due to less transmitted TE. In Figure 3 i), we can observe an overall increase of around 7.2 dB per 100 nm of gold at 10 THz. We can also conclude that COC polarizers present stable high broadband TM transmittance, while Si polarizers present loss in TM intensity with increased gold thickness. Nonetheless, as gold thickness increases the overall fabrication cost, depending on the application thinner thicknesses would be desirable without sacrificing ER much. For demonstration purposes in our fabricated polarizers, we limited Au thickness to 0.1 μm .

In summary, lower p , and higher d and t is desired for higher performance of DWGP as also previously predicted for Si.¹⁴ Higher impact on ER is obtain with higher t , followed by p and d , respectively. At 10 THz, we could observe a linear correlation with ER on COC devices: 72.0 dB/ μm of gold thickness, -8.8 dB/ μm of pitch and 2.5 dB/ μm of the depth. Similar values were found with Si devices at the same frequency. Overall, COC DWGP present superior performance when compared to Si with much higher TM, lower TE, and improved ER than the Si DWGP over the entire spectral range studied.

Fabrication of polarizers

Based on the simulation results in the last section, polarizers were fabricated in two materials, doped Si and COC with processes schematized in Figure 4. In both cases, the process starts by Direct Write Laser (DWL) patterning a grating over a photoresist layer on a Si substrate (Step 1), followed by transferring the pattern to Si by a dry etch process (Step 2) (section S5 of Supporting Information). An SF₆/C₄F₈ plasma in an inductively coupled plasma reactive ion etching (ICP – RIE) tool (Pegasus from SPTS) is used to open grooves 2 μm or 3 μm deep in the Si substrate. The resist mask is then stripped (Step 3) with an oxygen plasma asher (PVA GI-Gabatch 360 M from Tepla). From this point on, the Si and the COC processes diverge. For Si DWGP, Si dies (30 mm x 30 mm) are diced with alignment marks (Disco DAD 3500) to have good alignment in the FTIR system (section S6 of Supporting Information), and a 100 nm modified gold deposition (Step 4a) is performed on a confocal sputtering tool (Kenosistec Sputtering). To guarantee high anisotropy sputtering in this equipment, the sample holder is tilted 15° towards the sputtering target to compensate for the default system angle and the sample's rotation is disabled during the deposition process (section S7 of Supporting Information).

For the COC DWGP fabrication, after Step 3, Si molds are treated with an anti-sticking solution (Step 4b) before contact with polymer in a nanoimprint system (Obducat Eitre 8) (Step 5b).³¹ The patterned COC sheet is removed at demolding temperature of 50°C after the soft lithography process (section S8 of Supporting Information). The polymer sheet is diced through alignment marks imprinted in the material before following the same gold deposition as with Si substrates (Step 6b).

Two polarizers of each type were fabricated. Si polarizers were fabricated from doped Si with $p = 2 \mu\text{m}$, $d = 2 \mu\text{m}$, while COC polarizers were fabricated with $p = 2$ and 3 μm and $d = 3 \mu\text{m}$. All samples had a 100 nm of thin-film gold deposition. Perspective SEM images of Si and a COC polarizer are depicted in Figure 4c) and 4d), respectively (section S9 of Supporting Information). Several 2 mm-thick aluminum plaques were milled using a computer numerical control (CNC) system (FlexiCam Viper) in the shape of a rectangular mounting support, with a thinner bevelled edge region in the centre, to accommodate the polarizers at a fixed angle relative to the vertical, as depicted in Figure 4b) (section S10 of Supporting Information). Supports with the central regions making angles of 0°, 30°, 45°, and 60° were milled for an accurate positioning of the polarizers in the FTIR equipment.

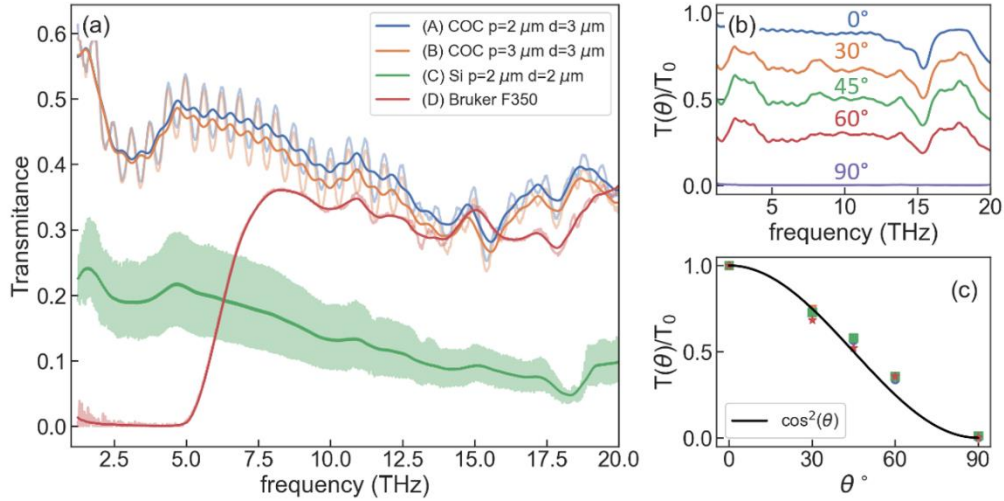


Figure 5. (a) Transmitted intensity of single polarizers: A) COC $p = 2 \mu\text{m}$, $d = 3 \mu\text{m}$ (blue), B) COC $p = 3 \mu\text{m}$, $d = 3 \mu\text{m}$ (orange), C) Si $p = 1 \mu\text{m}$, $d = 2 \mu\text{m}$ (green), and, D) commercial F350 polarizer from Bruker (red). Gold thickness for Si and COC polarizes are $0.1 \mu\text{m}$. (b) Normalized transmittance of COC $p = 2 \mu\text{m}$, $d = 3 \mu\text{m}$ as a function of relative polarizers' angles Θ , and, (c) the corresponding fitting curves to $\cos^2 \Theta$ at 10 THz.

Optical characterization

We characterized the polarization performance of fabricated polarizers in FTIR equipment with a Far-IR input source in transmission mode. Four different polarizers were inspected: A) COC $p = 2 \mu\text{m}$, $d = 3 \mu\text{m}$, B) COC $p = 3 \mu\text{m}$, $d = 3 \mu\text{m}$, C) Si $p = 1 \mu\text{m}$, $d = 2 \mu\text{m}$, and, D) a commercial polarizer from Bruker (F350). As observed in Figure 5 a), transmitted light from both COC polarizers outperforms both Si polarizers and commercial polarizer. At least double the transmitted polarized light is obtained in COC when compared to Si ones. This is particularly important and useful in many THz systems and applications due to low amplitude of radiation employed. Lower pitch COC polarizers ($p = 2 \mu\text{m}$) have slightly higher transmission than larger pitch ($p = 3 \mu\text{m}$), which is in good agreement with the simulation results. Si polarizers show less than half the transmission of COC polarizers as seen also in bulk materials transmission in Figure 2. Commercial polarizer performs very well at higher frequencies, however, its transmission falls at lower frequencies ($< 7.5 \text{ THz}$). Since light from the FTIR source is not polarized, a set of experiments was performed with two polarizers at different relative angles (0° , 30° , 45° , 60° , 90°) to study the performance of the fabricated polarizers. According to Malus' law, the transmittance intensity, T , should follow a function of polarizer relative angle, θ , $T(\theta) = T_0 \cos^2 \theta$, where $T_0 = T(0^\circ)$ is the initial transmittance of a single polarizer. To this purpose, one COC polarizer (A: $p = 2 \mu\text{m}$, $d = 3 \mu\text{m}$, $t = 0.1 \mu\text{m}$) was mounted in the FTIR equipment, and background measurement of the light transmitted by this polarizer was recorded - T_0 . Figure 5 b) shows the average light transmission of an additional COC polarizer (A: $p = 2 \mu\text{m}$, $d = 3 \mu\text{m}$, $t = 0.1 \mu\text{m}$) at different relative angles to the first. At $\theta = 0^\circ$, we can see a maximum transmission with a slight signal decrease in transmission due to material damping. The transmission of this device at $\theta = 0^\circ$ represents the transmitted TM of the polarizer. At $\theta = 90^\circ$, transmitted light close to zero is observed as expected when measuring two crossed polarizers. The transmission at an angle of $\theta = 90^\circ$ represents the transmitted TE. As observed in Figure 5 b), the transmission decreases for all frequencies with increasing angle θ until it reaches a minimum at 90° , confirming that the polarizers work over a broadband range of 0.9 - 20 THz. Taking always T_0 from the same COC polarizer (A: $p = 2 \mu\text{m}$, $d = 3 \mu\text{m}$), transmission as a function of θ was measured with other polarizers fabricated with COC (B: $p = 3 \mu\text{m}$, $d = 3 \mu\text{m}$), and, Si (C: $p = 1 \mu\text{m}$,

$d = 2 \mu\text{m}$) and, D, commercial Bruker F350. A fitting to Malus' law was done at 10 THz for all polarizers, and the results are shown in Figure 5 c). We confirm that all polarizers follow Malus' law indicating the high quality of fabricated DWGP. To evaluate the extinction ratio from our Si and COC DWGPs and commercial polarizer, TM and TE were acquired, as explained above, with the polarizers at angles $\theta = 0^\circ$ and $\theta = 90^\circ$. Again, the best performing COC polarizer (A: $p = 2 \mu\text{m}$, $d = 3 \mu\text{m}$, $t = 0.1 \mu\text{m}$) was used to produce the incident polarized beam.

DISCUSSION

Material selection for THz region is of critical importance particularly when designing both passive and active components. Here we showed for the first time a larger spectrum transmittances for two Si samples, doped and undoped, and two uprising class of cheaper materials with enhanced optical properties for this regime. Bulk materials transmittances in Figure 2 show an average increase of 35% for polymers when compared Si substrates.

Simulation results from Figure 3 show that polarizers fabricated on COC and doped substrates show distinguished performance and that COC polarizers surpass in both transmitted intensity and extinction ratio. Nanoimprinted process was developed to obtain COC DWGPs and was compared to Si DWGPs, with very low pitches compared to the literature. All fabricated polarizers and commercial polarizers followed Malu's law as shown in Figure 5 b) and c).

Figure 6 shows the TM light transmission of the four polarizers, with T_0 obtained with the polarizer (A) at $\theta = 0^\circ$. We can observe an overall intensity decrease from all polarizers, mainly due to substrate absorbance or reflections. COC polarizers show higher transparency over the full broadband range, with lower pitch (A) performing better than larger pitch polarizers (B). The commercial polarizer shows lower average transmission for higher frequencies and a cut-off below 7.5 THz. Si polarizers work on the full range, but they are much less transparent than COC polarizers and simulated TE show higher values. Our COC polarizers shows particularly superior transparency of at least doubled transmitted TM intensity when compared to Si ones.

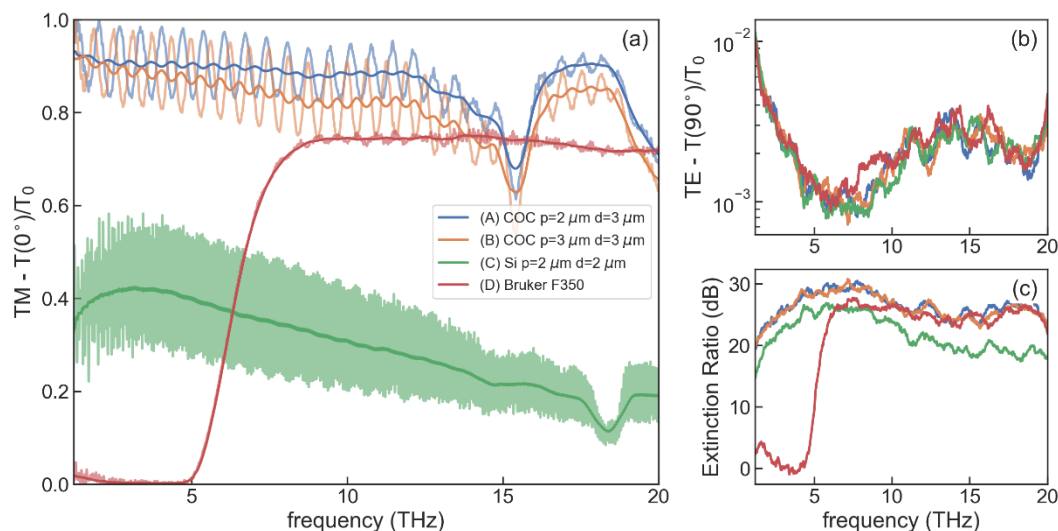


Figure 6. (a) Transmitted intensity of polarized light by single polarizers, $T(0^\circ)/T_0$: A) COC $p = 2 \mu\text{m}$, $d = 3 \mu\text{m}$ (blue), B) COC $p = 3 \mu\text{m}$, $d = 3 \mu\text{m}$ (orange), C) Si $p = 1 \mu\text{m}$, $d = 2 \mu\text{m}$ (green), and, D) commercial polarizer from Bruker (red). Gold thickness for Si and COC polarizers are $0.1 \mu\text{m}$. (b) Averaged TE transmittance in crossed configuration $T(90^\circ)/T_0$ for same polarizers. (c) Calculated extinction ratio for all polarizers.

Polarizer TE measurements were made with configuration ($\theta = 90^\circ$), and a moving window geometric mean was calculated to decrease noise fluctuations. The results are shown in Figure 6 b) for each polarizer. Here it's observed that TE intensity is very similar for all polarizers, and therefore we concluded that the obtained TE signals are mostly due to noise from the detector in FTIR equipment. Following the simulation predictions in Figure 3 d,e,f) The expected transmission intensity is below 10^{-4} , values much smaller than measured in Figure 6 b). The FTIR technique presents limitations on acquiring low TE transmission from polarizers when compared to other works that employ THz-TDS systems. This fact limits the possibility of obtaining accurate values of ER for such devices. Even so ER of around 25 dB indicate that for every transmitted TM intensity a proportional 0.3% of undesirable TE would be transmitted. This low intensity in practice is more than satisfactory for most applications. To further assess the ER of our polarizers, THz-TDS should be performed as this technique allows the detection of very low intensity transmitted TE. However, the spectral range is decreased to a smaller spectral band, typically in the range of 0.1 – 3 THz. We can assume that the real ER is higher than depicted in Figure 6 c), obtained from measured TM and TE of Figure 6a) and b). We can also observe that COC polarizers present an average increase of at least 4.4 dB in ER over the full range when compared to Si ones. As ER is proportional to the ratio TM/TE and COC polarizers present higher TM transparency, we can determine that COC polarizers present superior performance with higher ER than both Si and commercial Bruker polarizers in this full range. This fact is likewise shown predicted values from Figure 3 g,h,i).

Furthermore, the ER of these polarizers can easily be improved by increasing the thickness of the gold layer. The highest reported ER from a single DWGP Si polarizers of around 69.9 dB was achieved at 1.67 THz and thick Au layer of $0.4 \mu\text{m}$ ($p = 4 \mu\text{m}$, $d = 5 \mu\text{m}$).^{3,14} As shown from simulations, thicker gold layer has a higher impact on ER followed by smaller pitches and higher depth of trenches. Using the COC substrate with lower pitch, as we showed, would require less gold thickness to obtain reported ER for Si DWGP, leading to overall decrease costs associated with this step. Other benefits from our fabricated polarizers are the fact that they could be fabricated in roll-to-roll processes with lower cost polymer material and additional advantages of flexible substrate which could be integrated in curved surfaces.¹³ An additional fabrication option

to highly increase ER would be integrating two polarizers in the same COC sheet by nanoimprinting and gold sputtering on both sides, as previously demonstrated with Si polarizers.¹⁵ In this way, if both polarizers are close and aligned in the same film, this would minimize losses due to scattering and absorption by the optical medium in between them. This allows the use of one substrate with performance of two polarizers and thus achieving much higher ER.

CONCLUSION

In summary, we have experimentally demonstrated new broadband polarizers composed of a double wire grid made of thin-film gold on a transparent and flexible material such as a cyclic olefin copolymer. The COC polarizers were fabricated by nanoimprint soft lithography with a subwavelength pitch of 2 or 3 μm and depth of 3 μm . These results were compared to polarizers fabricated with Si substrate. Transmission spectra was recorded on a large broadband range 0.9 - 20 THz in an FTIR spectrophotometer not explored in past works and show that COC polarizers have more than doubled TM light transmission when compared to Si polarizers. COC and Si polarizers' performance matches the simulated analytical characteristics. COC polarizers showed exceptional performance below the 8 THz range when compared to Si and a commercial polarizer. Extinction ratio of COC polarizers present at least 4.4 dB increase when compared to similar geometry composed of Si material. This work proves that COC materials have superior performance in the THz range and would be very useful in many THz systems and applications, which can be easily up-scaled with lower fabrication costs and flexible material.

Supporting Information

The Supporting Information is available free of charge on the ACS Publications website. There are 10 sections regarding materials experimental procedures: Materials; Far-infrared characterization; Fringe smoothing; Simulations of double wire grid polarizers; Patterning, Reactive Ion Etching (RIE) process and Plasma Asher; Dicing dies; Modified Gold deposition; Nanoimprint process; Scanning Electron Microscopy; and, Holder for polarizers. (PDF)

AUTHOR INFORMATION

Corresponding Author

Alexandre Chicharo - International Iberian Nanotechnology Laboratory, Av. Mestre José Veiga SN, 4715-330, Braga, Portugal
Email: alexandre.chicharo@inl.int

Authors

Tatiana G. Rappoport - Instituto de Telecomunicações, Instituto Superior Técnico, University of Lisbon, Avenida Rovisco Pais 1, Lisboa, 1049-001 Portugal

Chun-Da Liao†, Jérôme Borme - International Iberian Nanotechnology Laboratory, Av. Mestre José Veiga SN, 4715-330, Braga, Portugal

Nuno M. R. Peres, Pedro Alpuim - International Iberian Nanotechnology Laboratory, Av. Mestre José Veiga SN, 4715-330, Braga, Portugal & Center of Physics, University of Minho, 4710-057, Braga, Portugal

Present Addresses

† Present address: National Taiwan University, Taipei 10617, Taiwan

Notes

The authors declare no competing financial interest.

ACKNOWLEDGMENT

This work was supported from Portuguese Foundation for Science and Technology (FCT) through projects GRAPHSENS (POCI-01-0145-FEDER-028114; PTDC/FISMAC/28114/2017) and TARGET (UTA-EXPL/NPN/0038/2019). TGR acknowledges funding from Instituto de Telecomunicações - grant number UID/50008/2020 in the framework of the project Sym-Break.

REFERENCES

- (1) Lewis, R. A. A Review of Terahertz Sources. *J. Phys. D. Appl. Phys.* **2014**, *47* (37). <https://doi.org/10.1088/0022-3727/47/37/374001>.
- (2) Sizov, F. F. Brief History of THz and IR Technologies. *Semicond. Physics, Quantum Electron. Optoelectron.* **2019**, *22* (1), 67–79. <https://doi.org/10.15407/spqoe22.01.067>.
- (3) Cho, Y. T. Fabrication of Wire Grid Polarizer for Spectroscopy Application: From Ultraviolet to Terahertz. *Appl. Spectrosc. Rev.* **2018**, *53* (2–4), 224–245. <https://doi.org/10.1080/05704928.2017.1328427>.
- (4) Shiraiishi, K.; Higuchi, S.; Muraki, K.; Yoda, H. Silver-Film Subwavelength Gratings for Polarizers in the Terahertz and Mid-Infrared Regions. *Opt. Express* **2016**, *24* (18), 20177. <https://doi.org/10.1364/oe.24.020177>.
- (5) Ren, L.; Pint, C. L.; Arikawa, T.; Takeya, K.; Kawayama, I.; Tonouchi, M.; Hauge, R. H.; Kono, J. Broadband Terahertz Polarizers with Ideal Performance Based on Aligned Carbon Nanotube Stacks. *Nano Lett.* **2012**, *12* (2), 787–790. <https://doi.org/10.1021/nl203783q>.
- (6) Wojdyla, A.; Gallot, G. Brewster's Angle Silicon Wafer Terahertz Linear Polarizer. *Opt. Express* **2011**, *19* (15), 14099. <https://doi.org/10.1364/oe.19.014099>.
- (7) Hsieh, C.-F.; Lai, Y.-C.; Pan, R.-P.; Pan, C.-L. Polarizing Terahertz Waves with Nematic Liquid Crystals. *Opt. Lett.* **2008**, *33* (11), 1174. <https://doi.org/10.1364/ol.33.001174>.
- (8) Mok, C. L.; Chambers, W. G.; Parker, T. J.; Costley, A. E. The Far-Infrared Performance and Application of Free-Standing Grids Wound from 5 Mm Diameter Tungsten Wire. *Infrared Phys.* **1979**, *19* (3–4), 437–442. [https://doi.org/10.1016/0020-0891\(79\)90055-1](https://doi.org/10.1016/0020-0891(79)90055-1).
- (9) Farid, A.; Laurita, N. J.; Tehrani, B.; Hester, J. G.; Tentzeris, M. M.; Armitage, N. P. Inkjet Printed Wire-Grid Polarizers for the THz Frequency Range. *J. Infrared, Millimeter, Terahertz Waves* **2017**, *38* (3), 276–282. <https://doi.org/10.1007/s10762-016-0330-5>.
- (10) Lai, W.; Yuan, H.; Fang, H.; Zhu, Y.; Wu, H. Ultrathin, Highly Flexible and Optically Transparent Terahertz Polarizer Based on Transparent Conducting Oxide. *J. Phys. D. Appl. Phys.* **2020**, *53* (12). <https://doi.org/10.1088/1361-6463/ab651c>.
- (11) Yamada, I.; Takano, K.; Hangyo, M.; Saito, M.; Watanabe, W. Terahertz Wire-Grid Polarizers with Micrometer-Pitch Al Gratings. **2009**, *34* (3), 274–276.
- (12) Cetnar, J. S.; Middendorf, J. R.; Brown, E. R. Extraordinary Optical Transmission and Extinction in a Terahertz Wire-Grid Polarizer. *Appl. Phys. Lett.* **2012**, *100* (23), 1–4. <https://doi.org/10.1063/1.4724315>.
- (13) Ferraro, A.; Zografopoulos, D. C.; Missori, M.; Peccianti, M.; Caputo, R.; Beccherelli, R. Flexible Terahertz Wire Grid Polarizer with High Extinction Ratio and Low Loss. *Opt. Lett.* **2016**, *41* (9), 2009. <https://doi.org/10.1364/ol.41.002009>.
- (14) Deng, L. Y.; Teng, J. H.; Zhang, L.; Wu, Q. Y.; Liu, H.; Zhang, X. H.; Chua, S. J. Extremely High Extinction Ratio Terahertz Broadband Polarizer Using Bilayer Subwavelength Metal Wire-Grid Structure. *Appl. Phys. Lett.* **2012**, *101* (1), 1–5. <https://doi.org/10.1063/1.4729826>.
- (15) Lu, B.; Wang, H.; Shen, J.; Yang, J.; Mao, H.; Xia, L.; Zhang, W.; Wang, G.; Peng, X. Y.; Wang, D. A High Extinction Ratio THz Polarizer Fabricated by Double-Bilayer Wire Grid Structure. *AIP Adv.* **2016**, *6* (2). <https://doi.org/10.1063/1.4942515>.
- (16) Neu, J.; Schmittenmaer, C. A. Tutorial: An Introduction to Terahertz Time Domain Spectroscopy (THz-TDS). *J. Appl. Phys.* **2018**, *124* (23). <https://doi.org/10.1063/1.5047659>.
- (17) Ren, L.; Pint, C. L.; Booshehri, L. G.; Rice, W. D.; Wang, X.; Hilton, D. J.; Takeya, K.; Kawayama, I.; Tonouchi, M.; Hauge, R. H.; Kono, J. Carbon Nanotube Terahertz Polarizer. *Nano Lett.* **2009**, *9* (7), 2610–2613. <https://doi.org/10.1021/nl900815s>.
- (18) Adams, J. L.; Botten, L. C. Double Gratings and Their Applications as Fabry-Perot Interferometers. *J. Opt.* **1979**, *10* (3), 109–117. <https://doi.org/10.1088/0150-536X/10/3/002>.
- (19) Goebel, T.; Schoenherr, D.; Sydlo, C.; Roggenbuck, A.; Deninger, A.; Meissner, P.; Hartnagel, H.-L. Tunable Fabry-Perot THz Filter with Sub-Wavelength Grating Mirrors. *Photonic Cryst. Mater. Devices VIII* **2008**, *6989* (November 2014), 698911. <https://doi.org/10.1117/12.781127>.
- (20) Sun, L.; Lv, Z. H.; Wu, W.; Liu, W. T.; Yuan, J. M. Double-Grating Polarizer for Terahertz Radiation with High Extinction Ratio. *Appl. Opt.* **2010**, *49* (11), 2066–2071. <https://doi.org/10.1364/AO.49.002066>.
- (21) Tydex. THz Materials. **2019**, 0–3.
- (22) Chandler-Horowitz, D.; Amirtharaj, P. M. High-Accuracy, Midinfrared (450 Cm⁻¹ ≤ ω ≤ 4000 Cm⁻¹) Refractive Index Values of Silicon. *J. Appl. Phys.* **2005**, *97* (12). <https://doi.org/10.1063/1.1923612>.
- (23) Rogalin, V. E.; Kaplunov, I. A.; Kropotov, G. I. Optical Materials for the THz Range. **2018**, *125* (6), 1053–1064. <https://doi.org/10.1134/S0030400X18120172>.
- (24) Cunningham, P. D.; Valdes, N. N.; Vallejo, F. A.; Hayden, L. M. Broadband Terahertz Characterization of the Refractive Index and Absorption of Some Important Polymeric and Organic Electro-Optic Materials Broadband Terahertz Characterization of the Refractive Index and Absorption of Some Important Polymeric and Organic. **2011**, No. May. <https://doi.org/10.1063/1.3549120>.
- (25) Angelo, F. D.; Mics, Z.; Bonn, M.; Turchinovich, D. Ultra-Broadband THz Time-Domain Spectroscopy of Common Polymers Using THz Air Photonics. **2014**, *22* (10), 2924–2926. <https://doi.org/10.1364/OE.22.012475>.
- (26) ZEON. Cyclo Olefin Polymer (COP) New high-performance thermoplastics for next-generation http://www.zeon.co.jp/business_e/enterprise/speplast/zeonex_e_201001.pdf.
- (27) TOPAS. Cyclic Olefin Copolymer (COC) TOPAS Product brochure https://topas.com/sites/default/files/files/topas_product-

- brochure_english.pdf.
- (28) Greivenkamp, J. E. *Field Guide to Geometrical Optics*; SPIE, Ed.; 2004; Vol. FG01.
- (29) Moellering, R.A., Bauer, L. B. & B. Epitaxial Layer Thickness Measurements Using Fourier Transform Infrared Spectroscopy (FTIR). *JEM* **1990**, *19* (2), 181–185. <https://doi.org/doi.org/10.1007/BF02651743>.
- (30) Shiraishi, K.; Muraki, K. Metal-Film Subwavelength-Grating Polarizer with Low Insertion Losses and High Extinction Ratios in the Terahertz Region. *Opt. Express* **2015**, *23* (13), 16676. <https://doi.org/10.1364/oe.23.016676>.
- (31) Galand, R.; Beaurain, A.; Francone, A.; Pelissier, B.; Zelsmann, M.; Boussey, J. Microelectronic Engineering Mold Cleaning and Fluorinated Anti-Sticking Treatments in Nanoimprint Lithography. *Microelectron. Eng.* **2009**, *86* (4–6), 669–672. <https://doi.org/10.1016/j.mee.2009.01.065>.